

Enhanced Photon Management of Thin-Film Silicon Solar Cells Using Inverse Opal Photonic Crystals with 3D Photonic Bandgaps

Leo T. Varghese, Yi Xuan, Ben Niu, Li Fan, Peter Bermel,* and Minghao Qi*

While silicon (Si) is the most widely used material for solar energy harvesting, it suffers from having an indirect bandgap, which dictates that a relatively thick Si material is required to absorb a significant portion of the solar spectrum. With cost a major concern for the photovoltaic industry, thinner films with enhancements in material efficiency are critical to drive down production costs. This is possible by increasing the path length of light in Si through the use of efficient light-trapping schemes.^[1]

Traditional optical path length enhancement is based on geometric optics through the use of texturing, which treats all wavelengths equally.^[2,3] An alternative approach based on wave optics is promising because it targets certain wavelengths in the near-IR, where it is most needed for Si. There has been extensive work in integrating plasmonics, gratings, and 1D distributed Bragg reflectors to improve light trapping.^[4–6] The use of 3D photonic crystals (PhCs) as back reflectors has been proposed for thin-film crystalline Si solar cells for their superior performance with just a few layers.^[7] Previous demonstrations using 3D PhCs as back reflectors were only performed on dye-sensitized solar cells,^[8,9] or as intermediate reflectors on tandem solar cells.^[10] Direct integration of 3D PhCs on crystalline Si solar cells as back reflectors has never been demonstrated due to the difficulties in incorporating PhCs with Si solar cells or the lack of high-quality PhCs targeting near-IR wavelengths.^[6]

In this work, we consider a novel experimental approach to improving the performance of thin-film (1.5 micrometer) crystalline silicon-based solar cells that combines the broadband response of textured light trapping with the optimally tailored design of photonic crystal-based light trapping structures. While the direct photonic bandgap of our inverse opal design is relatively modest, we also employ pseudogaps in the photon density of states for light incident from the sky to achieve strong reflection over the specific regions of the spectrum where light-trapping is most needed. Furthermore, the surface termination of our 3D photonic crystal is chosen specifically to optimize the probability of diffraction into guided modes that can be strongly

absorbed, as predicted by previous theoretical work.^[7] We find that the combination of reflection from photonic bandgap and pseudogap regions, diffuse back scattering, and periodic surface diffraction effects give rise to a significant performance advantage over plain aluminum back reflectors. By extension, most crystalline silicon thin film cells would be expected to see a similar set of benefits from our design approach.

Here, a 1.5 μm thick *p-i-n* Si solar cell is obtained from a vendor on a textured glass substrate. Si inverse opal PhCs are initially fabricated through a novel cleaning process that allows the opals to self assemble with minimum crack formation. We call it the S^5 process. Optical absorption measurements demonstrate that the use of Si inverse opal PhCs on the textured cells allows increased absorption at near-IR wavelengths. By self assembling on oxidized wafers, the inversion of the opal template after filling allows the generation of PhC membranes. These free-standing membranes can be readily transferred and still maintain good optical quality. After electrically contacting the textured cell from the back, the PhC membranes are integrated on the back to measure the efficiency improvement under AM 1.5 solar illumination. *I-V* measurements reveal a 10% improvement in efficiency with simulations of its photocurrent matching well with the experimental data. Further optimization in the thickness of the solar cell and PhC properties could provide an improvement of up to 35%.^[7]

The basic strategy is built on previous work with meniscus-driven silica opal self-assembly, followed by filling with silicon, and concluding with the etching of the original silica opal to produce an inverted structure with a 3D photonic bandgap. **Figure 1a–e** illustrates the S^5 process used to fabricate high-quality, self-assembled, 3D silica opal templates. The S^5 process includes the Stöber method, sintering, sedimentation, SC1 cleaning, and self assembly. This process begins with a modified Stöber method, used to generate monodisperse spheres with diameters of around 550 nm (Figure 1a).^[11,12] While these opals can readily be used to form a 3D opal template through self-assembly,^[13,14] it was observed in both our experiments and in the literature that cracks initially form on the opal crystals after meniscus-driven self-assembly due to drying.^[15] When interstitial spaces in the opal crystal are filled with a high-index material at elevated temperatures, necessary to obtain a complete photonic bandgap,^[16] shrinkage of the opals at such high temperatures leads to exaggerated cracks, leading to degraded optical performance. Fortunately, low defect-density 3D PhCs can be achieved by first sintering them (Figure 1b).^[17,18] However, this raises two issues. First, the diameter of the opals reduces by about 5–10% due to water loss and densification, which can easily be countered by synthesizing larger diameter

L. T. Varghese, Dr. Y. Xuan, B. Niu, L. Fan,
Prof. P. Bermel, Prof. M. Qi
Birck Nanotechnology Center and School of Electrical
and Computer Engineering
Purdue University
Indiana, 47907, USA
E-mail: pbermel@purdue.edu; mqj@purdue.edu



DOI: 10.1002/adom.201300254

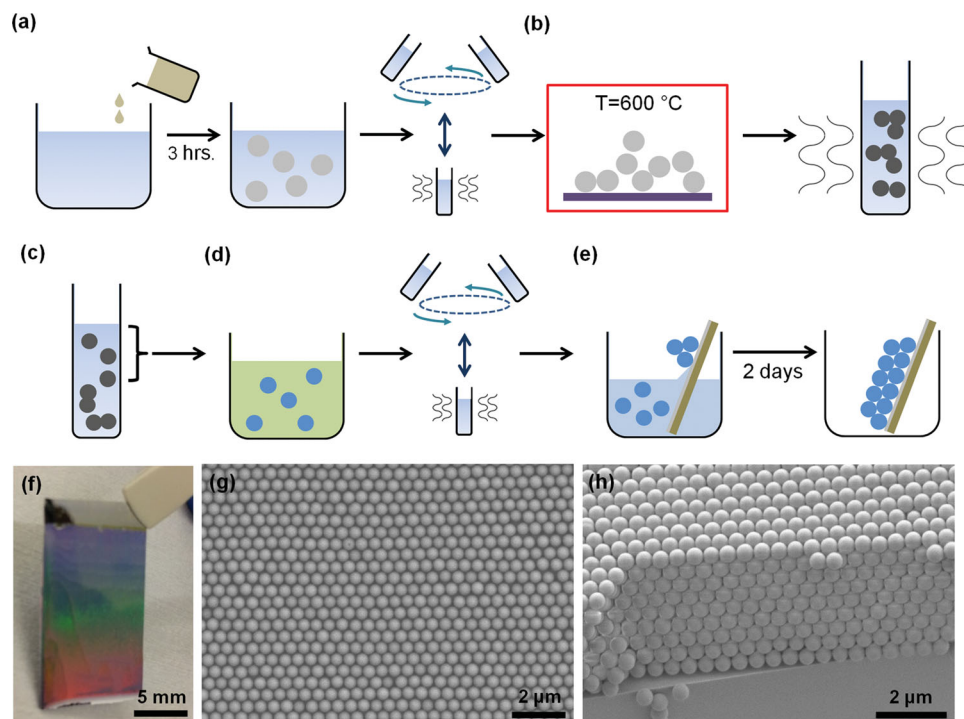


Figure 1. Self assembly process flow demonstrating the S^5 process. (a) Stöber method where tetraethyl orthosilicate is added to an ethanolic solution containing water and ammonium hydroxide. After 3 h, silica spheres are formed which are then repeatedly centrifuged and sonicated. (b) Sintering of opals in a furnace at 600 °C for 24 h followed by dispersing them in ethanol through sonication. (c) Gravity driven sedimentation to isolate aggregated opals. (d) SC1 clean followed by repeated centrifugation and sonication to remove the reactants. (e) Self assembly of opals on an oxide wafer through evaporation of solvent. (f) Optical image of the opals on a Si wafer. (g) Top view of the opals. (h) Side-view of the opals on a bare Si wafer.

opals. Second, sintering the opals in close proximity to neighboring opals encourages the formation of sinter necks,^[19] resulting in opal aggregates, which can severely impede self assembly. This is remedied by dispersing the opals in solvents for prolonged periods and allowing aggregates to settle through gravity-driven sedimentation (Figure 1c). While previous works on realizing crack-free PhCs used sintering and sedimentation only, we often found self assembling these opals to be unsuccessful.

However, we discovered that if the sintered and sedimented opals are cleaned in a solution containing ammonium hydroxide, hydrogen peroxide and water (SC1 clean) prior to self assembly (Figure 1d), these opals could form opal crystals relatively easily (Figure 1e). One possible explanation is that, in the sintering step, the hydrophilic surface of Stöber-synthesized opals turns hydrophobic at elevated temperatures due to the reduction of silanol bonds and the increase of siloxane bonds.^[20] With the SC1 clean able to etch oxide by a few angstroms per minute,^[21] it exposes the inner silanol bonds and essentially refreshes the opal's surface to its old state prior to the sintering process. It is therefore reasonable to hypothesize that the opal's hydrophilic nature may facilitate self assembly, since fluid flow is a driving factor for the formation of opal crystals.^[22]

Optical and scanning electron microscope (SEM) images of opal crystals after the S^5 process is shown in Figure 1f–h. For opals with a diameter around 500 nm, a 1% volume fraction yields between 8 and 12 layers. The reflection spectra of the

opal crystals, shown in Figure 2, demonstrates that the crystals assembled from the S^5 process have a strong and distinct peak dictated by Bragg's law,^[23] while the spectra of the film obtained

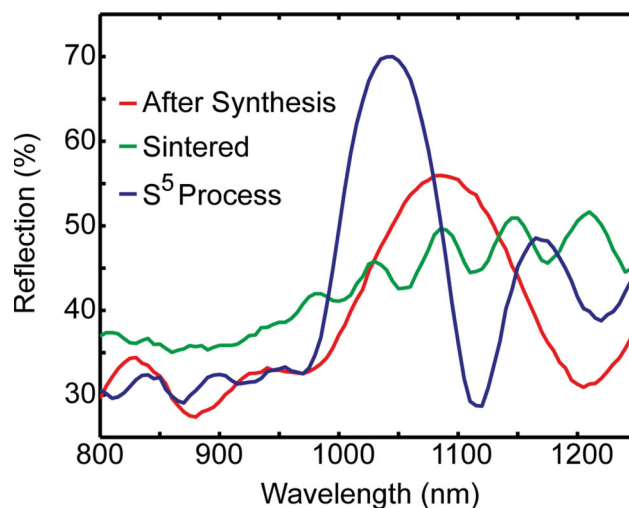


Figure 2. Optical spectra of various opals. Reflectivity spectra measured by assembling opals on a Si wafer. Note that the spectra of the opal crystals after S^5 process (blue) is shifted to smaller wavelengths compared to the opals after Stöber synthesis (red) which is attributed to the shrinkage of the opals. The spectra of the sintered opals (green) have a broad peak signifying disorder.

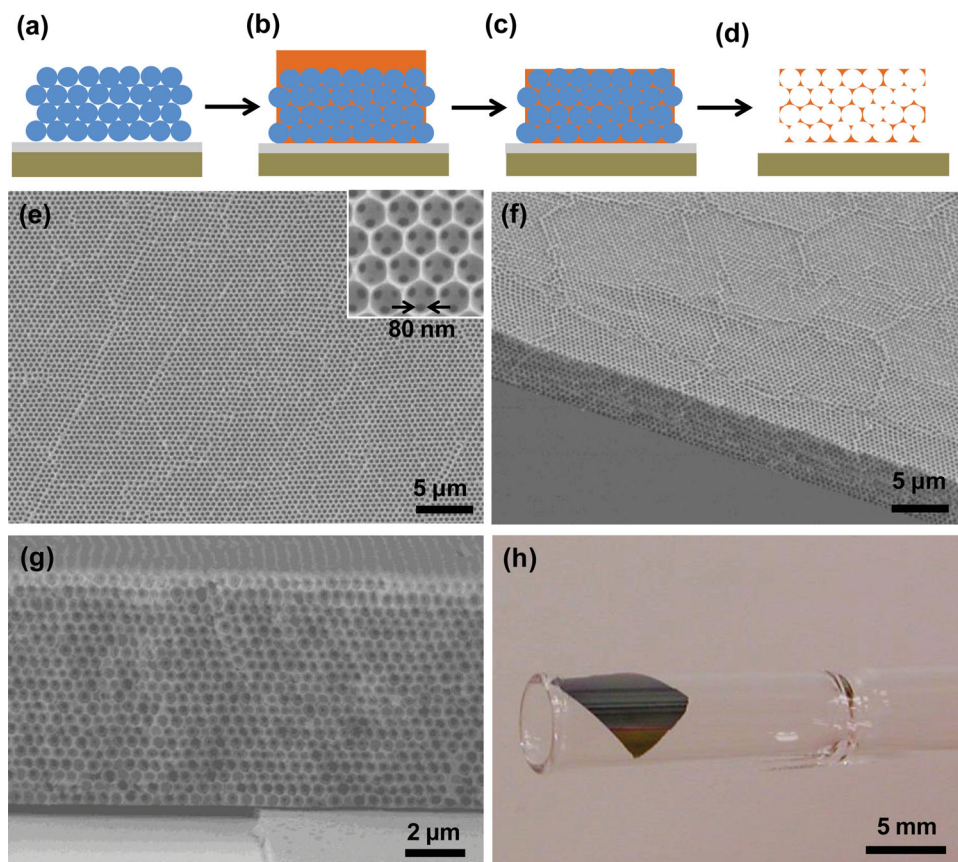


Figure 3. Formation and release of inverse opal PhCs. (a) Self assembled opal crystal on an oxide wafer. (b) Amorphous Si filling of opals using LPCVD. (c) RIE etching to expose the top opals. (d) Inversion in dilute HF acid to form the PhC membrane. (e) Top view SEM image after the removal of the opals with an inset showing the sinter-necks. (f) Tilted view SEM image of the inverse opal PhCs. (g) SEM image of a PhC membrane sitting over a metal contact. (h) Optical image of a PhC membrane wrapped around the head of a pipette.

from opals only experiencing sintering and sedimentation is weak with multiple peaks, indicating high disorder.

After self assembly (Figure 3a), the interstitial spaces are filled with amorphous Si using low pressure chemical vapor deposition (LPCVD; Figure 3b).^[24] This step results in a thin layer of amorphous Si over the opal crystal (Figure S1) which is etched away using Cl_2/Ar plasma (Figure 3c) through reactive-ion etching (RIE). To form inverse opal PhCs (Figure 3d), the sample is dipped in dilute hydrofluoric (HF) acid to remove the opals by the network of sinter necks (inset of Figure 3e). The top and side-view SEM images of the inverted PhCs are shown in Figure 3e and f, respectively. To lift off the PhCs from the substrate, the self assembly process is undertaken on an oxide wafer, which allows it to release as a membrane when dipped in HF. While the PhC membrane is rigid in the micrometer range (Figure 3g), it is flexible in the millimeter range (Figure 3h). A comparison of an inverse opal PhC assembled with opals obtained from Stöber synthesis and one from the S^5 process is shown in Figure S2. Without the S^5 process, released PhC membranes are fragile and can disintegrate easily when handled because of the large discontinuities in the crystal. Figure 4 is the total reflection spectrum of a PhC membrane sitting on a quartz wafer. The presence of distinct peaks around ~ 1050 nm and ~ 990 nm, which are the second and third reflection bands,

respectively, for an inverse opal PhC, demonstrates the high crystalline order of the opals.^[25] While the measured reflectivity is not very high in the NIR, this comes from residual defects

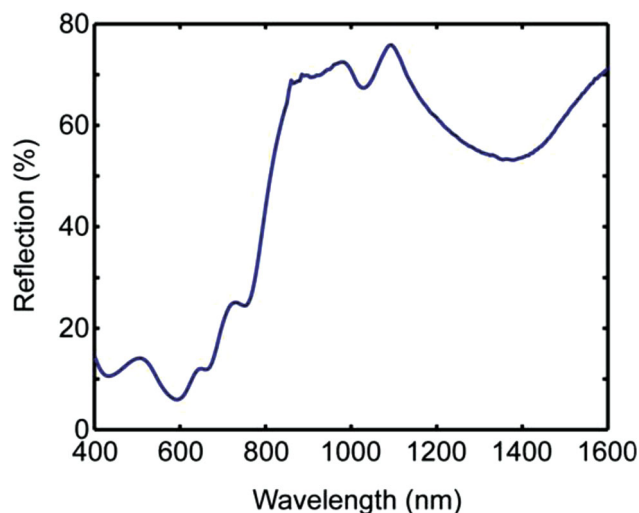


Figure 4. Total reflection spectrum of a PhC membrane on a quartz wafer. It includes specular and diffusive components.

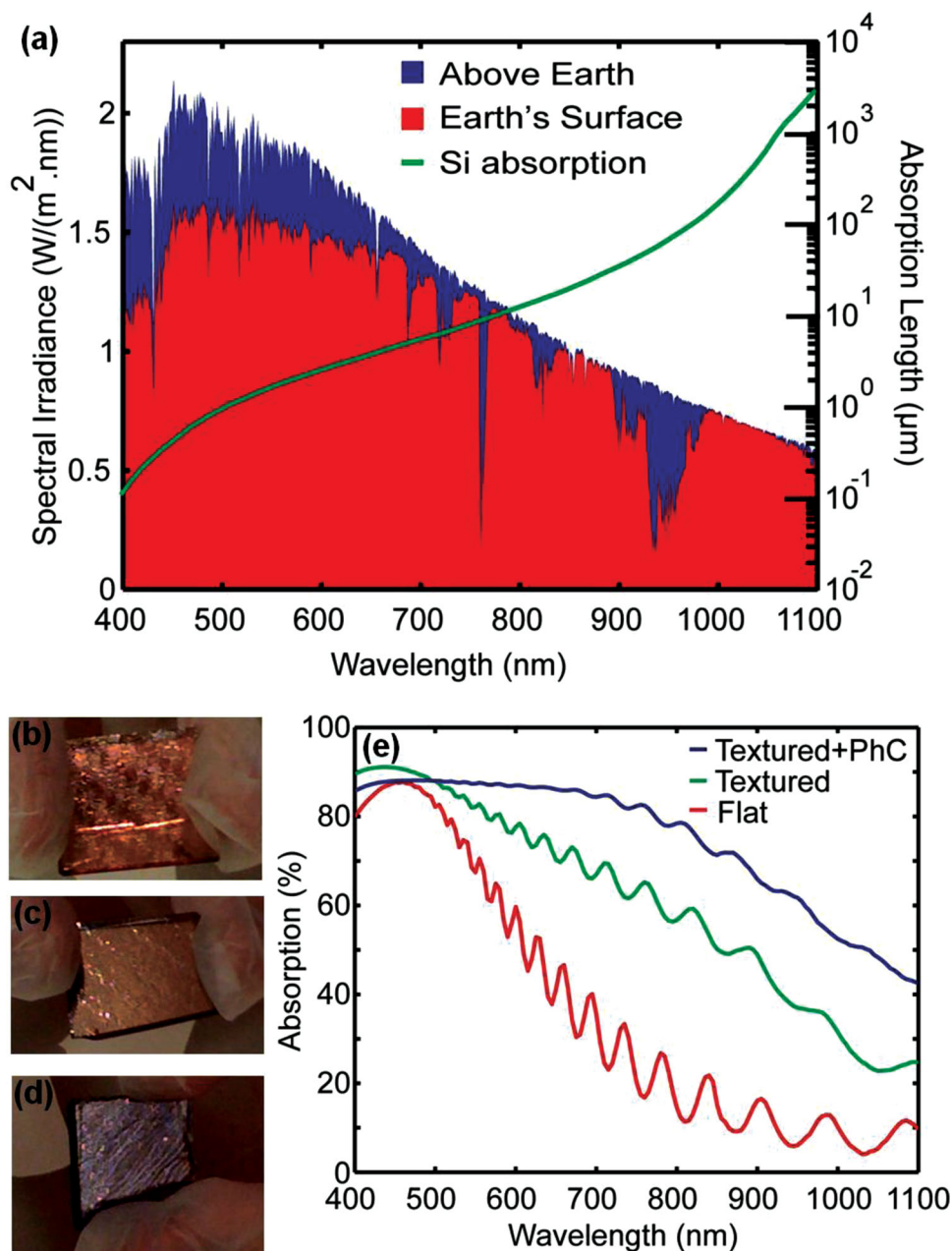


Figure 5. Optical performance of PhCs on thin-film Si solar cells. (a) Solar spectra (left y axis) AM0 (above the atmosphere, red) and AM1.5G (at sea level, blue). The absorption length of crystalline Si (right y axis) is overlaid. (b) A flat cell with no light trapping schemes observed to be shiny. (c) A textured cell. (d) A textured cell with a PhC at the back which is observed to be dark. (e) Absorption spectra of the cells shown in (b–d). The cells in (b–d) are approximately 2 cm × 2 cm.

in the assembly process. As such, we believe it causes diffuse back reflection, which benefits the cell. This combination of diffuse back reflection and diffraction effects gives rise to a significant amount of light trapping that gives an advantage over aluminum.

Figure 5a shows the solar spectrum overlaid with the absorption length of crystalline Si between 400 and 1100 nm.^[26,27] While the shorter wavelengths only require less than a micrometer thick Si to absorb most of the light, longer wavelengths are poorly absorbed. For example, to absorb a majority of the

solar irradiation with a wavelength of 800 nm, over 10 μm thick silicon is required. This is evident in Figure 5e which characterizes the absorption of various light trapping schemes for Si polycrystalline solar cells with 1.5 μm thickness. The ringing in the spectra is a result of the Fabry–Perot oscillations inside the thin film. Figure 3b shows a flat cell with only *p-i-n* layers on a smooth glass substrate and no light trapping schemes. As expected, it performs poorly for wavelengths beyond 600 nm (Figure 5e). For a textured cell with the same thickness (Figure 5c), the absorption of light in the NIR improves

due to light trapping based on geometric optics. When a PhC is fabricated on the backside of the textured cell (Figure 5d), the absorption is strongest, hence it looks darkest.

In order to measure the electrical performance of the solar cells with PhCs as back reflectors, initial attempts were made to make electrical contact to PhC backed solar cells. For example, self assembly of opal crystals were carried out directly on the backside of a textured cell and inverse opal PhCs were formed by filling and inversion. Finally, contacts were made on the backside of the cell by etching away sections of the PhC. However, this approach resulted in poor electrical performance because of the exposure of the solar cell to PhC fabrication conditions and handling. Also having both the PhC and metal contacts on the backside of the cell led to complex integration issues.

Instead, we isolated the two fabrication processes: the cells are electrically contacted and at the same time, PhCs are formed on an oxide wafer for transfer to an electrically contacted cell. Not only does this simplify processing for the two processes, it also limits the thermal budget and contamination of the solar cell while allowing high quality crystals to assemble on flat substrates. The metal contacting scheme is shown in Figure S3. In this approach, a mesa structure is first formed by photolithography and wet etching of poly-silicon with a solution containing potassium permanganate and dilute HF. Since the etching step needs to stop at the $n+$ region, a thicker $n+$ region is used in this prototyping study, although it reduces the external quantum efficiency (EQE). Oxide is next deposited and aluminum metal contacts are evaporated and patterned through lift-off. Figure 6a is an optical image of the back of an electrically contacted solar

cell. A free-standing PhC membrane (Figure 2g,h) is transferred to an electrically contacted cell through water assisted transfer and placed over the mesa, enveloping the metal finger contact for $p+$, and allowed to air dry.

Electrical characterizations of the textured cells are performed under AM1.5 solar illumination. After I - V measurements are obtained for textured cells with a PhC backing, the PhC is removed to measure the textured cell as a reference under identical conditions. A different textured cell with a 100 nm Al metal backing is measured for comparison. Figure 6b is an I - V measurement where a short-circuit current density (J_{sc}) of 13.4 mA/cm² is observed for a textured cell with an open circuit voltage (V_{oc}) of 0.39 V and fill factor (FF) of 0.58. When a PhC is used as a back reflector for the same cell, J_{sc} jumps to 14.7 mA/cm² ($V_{oc} = 0.39$ V, $FF = 0.59$), a J_{sc} enhancement of 9.6%. A metal backed textured cell has a J_{sc} of 14.2 mA/cm² ($V_{oc} = 0.39$ V, $FF = 0.58$), a J_{sc} enhancement of 6.0% compared to the reference. In terms of efficiency, the PhC backed cell performs the best with an improvement of 10.66%. Here, the enhancement in the EQE spectrum for the cells (Figure 6c) is obtained by taking the ratio of the absorption spectrum for textured cells compared to flat cells, as well as the ratio of the absorption spectrum for textured cells with photonic crystals compared to flat cells. It is evident that adding the photonic crystal features results in a greater EQE enhancement overall. Using an S-matrix method and a haze factor to account for a textured solar cell, $dJ_{sc}/d\lambda$ is calculated as shown in Figure 6d. By integrating this curve, a J_{sc} enhancement of 6% is calculated for a non-ideal Al metal backing,^[7] compared to a cell

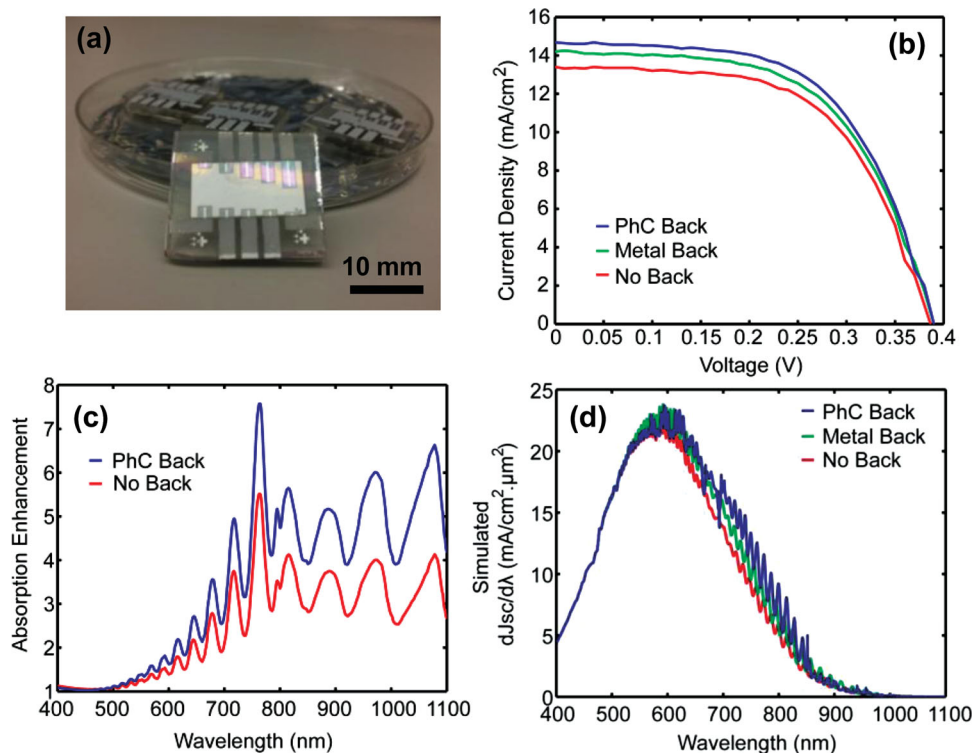


Figure 6. Characterization of the solar cell. (a) Optical image of the electrical contacts on the backside of the solar cell. (b) I - V measurements under AM1.5 solar illumination for the textured cells. (c) Calculated enhancement in the external quantum efficiency spectrum for the textured solar cells. (d) Simulated $dJ_{sc}/d\lambda$ versus wavelength for the textured cells.

with no backing, and 9% for a 15 layer ideal inverse opal PhC with an opal diameter of 500 nm. The simulated J_{sc} enhancements match reasonably well with the experimental data and are within the uncertainties of the simulation parameters.

To our knowledge, this is the first demonstration of incorporating 3D PhCs to increase light trapping in crystalline Si solar cells. A number of challenges were met which led to only modest improvement in experimental efficiencies. First, the use of a 200 nm $n+$ region to allow ease in contacting from the back led to increased free carrier absorption. With better control in the wet etching, a thinner $n+$ layer would substantially increase the generation of an electron-hole pairs and obtain higher baseline efficiencies. Second, the use of textured cells and a metallic finger for the $p+$ contact compromised the performance of the PhC since an inevitable air gap is present between the cell and the PhC. While a possible solution is to self assemble on the textured topography of the solar cell and form the PhC, this approach led to poor electrical performance as discussed earlier. Improved performances are possible by both contacting from the front and allowing the PhC to occupy the backside completely, or by first generating the PhC prior to the deposition of solar cell material. Also, with the use of an effectively thinner cell and optimization of the PhC's optical properties, a 35% enhancement in J_{sc} is theoretically possible.^[7] The use of inverse opal PhC demonstrated here could also modify the Shockley–Queisser limit leading to improved electrical performance.^[28]

In conclusion, we have employed a novel S^5 process of ensuring the self assembly of opals and its transformation into Si inverse opal PhCs formed crack-free structures with minimal defects. The optical performance of Si inverse opal PhCs as back reflectors for Si solar cells are experimentally demonstrated, showing increased absorption of near-IR wavelengths. Using free-standing PhC membranes that are transferred onto electrically contacted cells, it decouples the fabrication of the two processes, simplifying integration. Solar measurements indicate that the use of PhC has a 10% enhancement in short circuit current, matching well with simulation calculations. With higher short circuit current enhancement possible with optimized designs, and no corresponding degradation in open-circuit voltage V_{oc} or the fill factor, the use of 3D PhCs to increase material efficiencies for Si solar cells holds great promise for further research.

Experimental Section

S^5 Process, Filling, and Inversion: Stöber synthesized opals were dried in air and sintered in a horizontal furnace at 600 °C in N_2 for 24 h. After sedimentation, highly monodisperse opals were cleaned in a solution containing ammonium hydroxide, hydrogen peroxide and water ($NH_4OH: H_2O_2: H_2O = 1:1:6$) at 70 °C for 5 min. A Si wafer with 300 nm oxide was cleaned in solution containing sulfuric acid and hydrogen peroxide ($H_2SO_4: H_2O_2 = 1:1$) for 10 min. The cleaned wafer was dipped in an ethanolic suspension containing the opals at an angle of $\sim 45^\circ$. The apparatus was placed in a temperature controlled incubator with a temperature of ~ 28 °C on an optical table. Amorphous silicon was deposited in low pressure chemical vapor deposition (LPCVD) using silane (SiH_4) decomposed at 550 °C. A blanket Cl_2/Ar reactive-ion etching (RIE) was used expose the top opal after which it was dipped in 5% dilute HF to remove the opals and form a Si inverse opal PhC.

Solar Cell Metallization: A ~ 1.5 μm thick p - i - n polycrystalline Si solar cell with and without texturing was received from a commercial vendor. The solar cell was on a ~ 3 mm substrate with a 90 nm silicon nitride layer, 200 nm $n+$ layer, 1.2 μm p - layer and 60 nm $p+$ layer. Contacting for $p+$ and $n+$ regions were performed from the backside only. Photolithography was used to pattern the active area using AZ9620 resist. The exposed regions were etched down to the $n+$ region using a solution containing potassium permanganate ($KMnO_4$) and dilute HF. Continuous agitation was required to get a uniform etch rate. After removing the resist, 2 μm silicon dioxide was deposited over the cell's surface to protect the sidewall. This was accomplished through LPCVD of SiH_4 and O_2 at 400 °C in a caged boat configuration. The deposited oxide was patterned through photolithography and etched in dilute HF. Plasma enhanced chemical vapor deposition (PECVD) was next used to deposit 130 nm oxide at 300 °C. Contacts and pads were defined by photolithography of AZ1518 resist which was briefly dipped in dilute HF to remove the PECVD oxide over the contact regions followed by a deposition of 5 nm titanium for adhesion and 200 nm thick aluminum. Lift-off was performed in acetone to remove the resist following by a rapid thermal anneal at 400 °C for 30 s to reduce contact resistance and make Ohmic contact between the metal pads and cells.

Absorption Measurement: A Lambda 950 UV-vis-NIR spectrophotometer was used for the absorption measurements. By illuminating the sample from the front at a near normal incidence of $\sim 10^\circ$, reflected and transmitted light was collected using a 150 mm integrating sphere.

Light Characterization: I - V measurements of the solar cell were performed under AM1.5 solar illumination using a custom made setup. I - V measurements were taken first with the PhC sitting on the back of the textured cell and then without it. The PhC was removed without physically moving the cell or the electrical probes through the use of compressed air. A different cell was used to measure the metal backed performance.

Simulation: The electrical performances of the various solar cells were studied via the S-matrix method,^[29,30] which calculates the coupling between incoming and outgoing waves for a finite dielectric structure. This method was implemented by a proprietary code developed by our research group, along similar lines as the freely available S4 tool developed by Shanhui Fan's group at Stanford.^[31] The structure was divided into a finite series of layers in the z -direction, each of which were assumed to have a uniform profile in that direction. Absorption was then calculated at each wavelength by subtracting the quotient of the total reflected and transmitted power (P_R and P_T , respectively) over the total incident power P_I from unity. The differential J_{sc} contribution can then be calculated as follows:

$$\frac{dJ_{sc}}{d\lambda} = \frac{q\lambda}{hc} \left[1 - \frac{P_R + P_T}{P_I} \right] = \frac{q\lambda}{hc} A(\lambda) \quad (1)$$

Dispersion was accounted for in the frequency-domain method by constructing a new dielectric function at each wavelength.

Supporting Information

Supporting Information is available from the Wiley Online Library or from the author.

Acknowledgements

We thank Professor H. Hillhouse for access to his solar measurement setup. We thank Dr. Maroof Khan for his help in the metallization of the solar cells. This was supported by the Bay Area PV Consortium, a Department of Energy project with Prime Award number DE-EE0004946, by Defense Threat Reduction Agency (DTRA) grants HDTRA1-07-C-0042 and HDTRA1-10-1-0106, Air Force Office of Scientific Research (AFOSR) grant FA9550-08-1-0379, National Institutes of Health grant 1R01RR026273-01, and National Science

Foundation grant CNS-1126688. M.Q. acknowledges partial support from CAS International Collaboration and Innovation Program on High Mobility Materials Engineering.

Received: June 15, 2013

Published online:

-
- [1] E. Yablonovitch, G. D. Cody, *IEEE Trans. Electr. Dev.* **1982**, 29, 300.
- [2] J. Muller, B. Rech, J. Springer, M. Vanecek, *Sol. Energy* **2004**, 77, 917.
- [3] J. Zhao, A. Wang, P. Altermatt, M. A. Green, *Appl. Phys. Lett.* **1995**, 66, 3636.
- [4] E. T. Yu, J. van de Lagemaat, *Mrs Bull.* **2011**, 36, 424.
- [5] V. E. Ferry, J. N. Munday, H. A. Atwater, *Adv. Mater.* **2010**, 22, 4794.
- [6] R. B. Wehrspohn, J. Upping, *J. Opt.* **2012**, 14.
- [7] P. Bermel, C. Luo, L. Zeng, L. C. Kimerling, J. D. Joannopoulos, *Opt. Express* **2007**, 15, 16986.
- [8] A. Mihi, C. J. Zhang, P. V. Braun, *Angew. Chem. Int. Edit.* **2011**, 50, 5711.
- [9] S. Nishimura, N. Abrams, B. A. Lewis, L. I. Halaoui, T. E. Mallouk, K. D. Benkstein, J. van de Lagemaat, A. J. Frank, *J. Am. Chem. Soc.* **2003**, 125, 6306.
- [10] J. Upping, A. Bielawny, R. B. Wehrspohn, T. Beckers, R. Carius, U. Rau, S. Fahr, C. Rockstuhl, F. Lederer, M. Kroll, T. Pertsch, L. Steidl, R. Zentel, *Adv. Mater.* **2011**, 23, 3896.
- [11] G. H. Bogush, M. A. Tracy, C. F. Zukoski, *J. Non-Cryst. Solids* **1988**, 104, 95.
- [12] W. Stober, A. Fink, E. Bohn, *J. Colloid Interface Sci.* **1968**, 26, 62.
- [13] H. Miguez, C. Lopez, F. Meseguer, A. Blanco, L. Vazquez, R. Mayoral, M. Ocana, V. Fornes, A. Mifsud, *Appl. Phys. Lett.* **1997**, 71, 1148.
- [14] P. Jiang, J. F. Bertone, K. S. Hwang, V. L. Colvin, *Chem. Mater.* **1999**, 11, 2132.
- [15] L. K. Teh, N. K. Tan, C. C. Wong, S. Li, *Appl. Phys. A—Mater.* **2005**, 81, 1399.
- [16] H. S. Sozuer, J. W. Haus, R. Inguva, *Phys. Rev. B* **1992**, 45, 13962.
- [17] A. A. Chabanov, Y. Jun, D. J. Norris, *Appl. Phys. Lett.* **2004**, 84, 3573.
- [18] S. A. Rinne, F. Garcia-Santamaria, P. V. Braun, *Nat. Photon.* **2008**, 2, 52.
- [19] J. S. King, D. P. Gaillot, E. Graugnard, C. J. Surnmers, *Adv. Mater.* **2006**, 18, 1063.
- [20] L. T. Zhuravlev, *Colloid Surf. A—Physicochem. Eng. Asp.* **2000**, 173, 1.
- [21] S. W. Lim, *Jpn. J. Appl. Phys.* **1 2003**, 42, 5002.
- [22] D. J. Norris, E. G. Arlinghaus, L. L. Meng, R. Heiny, L. E. Scriven, *Adv. Mater.* **2004**, 16, 1393.
- [23] J. F. Bertone, P. Jiang, K. S. Hwang, D. M. Mittleman, V. L. Colvin, *Phys. Rev. Lett.* **1999**, 83, 300.
- [24] Y. A. Vlasov, X. Z. Bo, J. C. Sturm, D. J. Norris, *Nature* **2001**, 414, 289.
- [25] T. Suezaki, P. G. O'Brien, J. I. L. Chen, E. Loso, N. P. Kherani, G. A. Ozin, *Adv. Mater.* **2009**, 21, 559.
- [26] ASTM G173–03, *Standard Tables for Reference Solar Spectral Irradiances: Direct Normal and Hemispherical on 37 degree Tilted Surface* (ASTM International, West Conshohocken, Pennsylvania, 2012).
- [27] M. A. Green, M. J. Keevers, *Prog. Photovoltaics* **1995**, 3, 189.
- [28] J. N. Munday, *J. Appl. Phys.* **2012**, 112, 6.
- [29] L. F. Li, *J. Am. Chem. Soc. A* **1996**, 13, 1024.
- [30] D. M. Whittaker, I. S. Culshaw, *Phys. Rev. B* **1999**, 60, 2610.
- [31] V. Liu, S. H. Fan, *Comp. Phys. Commun.* **2012**, 183, 2233.